New Phytologist

Research

Cell size influences inorganic carbon acquisition in artificially selected phytoplankton

Martino E. Malerba[1,2,6], Dustin J. Marshall[1,2], Maria M. Palacios[1,2], John A. Raven[3,4,5] and John Beardall[1]

[1]School of Biological Sciences, Monash University, Clayton, Vic. 3800, Australia; [2]Centre of Geometric Biology, Monash University, Clayton, Vic. 3800, Australia; [3]Division of Plant Sciences, University of Dundee at the James Hutton Institute, Invergowrie, Dundee DD2 5DA, UK; [4]Climate Change Cluster, University of Technology, Sydney, Ultimo, NSW 2007, Australia; [5]School of Biological Sciences, University of Western Australia, 35 Stirling Highway, Crawley, WA 2009, Australia; [6]Current address: School of Life and Environmental Sciences, Deakin University, Burwood, Vic. 3125, Australia

Author for correspondence:
Martino E. Malerba
Email: martino.malerba@gmail.com

Received: *20 May 2020*
Accepted: *2 November 2020*

New Phytologist (2020)
doi: 10.1111/nph.17068

Key words: CO_2-concentrating mechanisms, carbonic anhydrase, cell size, external carbonic anhydrase, green algae, inorganic carbon, photosynthetic O_2 evolution.

Summary

- Cell size influences the rate at which phytoplankton assimilate dissolved inorganic carbon (DIC), but it is unclear whether volume-specific carbon uptake should be greater in smaller or larger cells. On the one hand, Fick's Law predicts smaller cells to have a superior diffusive CO_2 supply. On the other, larger cells may have greater scope to invest metabolic energy to upregulate active transport per unit area through CO_2-concentrating mechanisms (CCMs).
- Previous studies have focused on among-species comparisons, which complicates disentangling the role of cell size from other covarying traits. In this study, we investigated the DIC assimilation of the green alga *Dunaliella tertiolecta* after using artificial selection to evolve a 9.3-fold difference in cell volume. We compared CO_2 affinity, external carbonic anhydrase (CA_{ext}), isotopic signatures ($\delta^{13}C$) and growth among size-selected lineages.
- Evolving cells to larger sizes led to an upregulation of CCMs that improved the DIC uptake of this species, with higher CO_2 affinity, higher CA_{ext} and higher $\delta^{13}C$. Larger cells also achieved faster growth and higher maximum biovolume densities.
- We showed that evolutionary shifts in cell size can alter the efficiency of DIC uptake systems to influence the fitness of a phytoplankton species.

Introduction

Cell volume spans seven orders of magnitude among phytoplankton species, from 0.1 μm^3 in picophytoplankton to 10^9 μm^3 in mesophytoplankton (Sieburth *et al.*, 1978; Beardall *et al.*, 2009; Finkel *et al.*, 2010). Because all organisms must conform to physical laws dictating the flow of resources, cell size determines physiological processes such as light harvesting, nutrient acquisition, cellular composition and, ultimately, growth. Cell size also influences physical processes (such as sinking) and ecological interactions (such as grazing; Finkel *et al.*, 2010). Given that around half of the net primary production on the planet originates from the oceans (Field *et al.*, 1998), understanding the effects of cell size on phytoplankton communities has been a major research topic for decades (Raven & Kübler, 2002; Raven *et al.*, 2005; Litchman & Klausmeier, 2008; Beardall *et al.*, 2009; Finkel *et al.*, 2010; Maranon, 2015).

Phytoplankton cells take up inorganic carbon either through diffusive CO_2 movement and catalysis of extracellular equilibration of HCO_3^- and CO_2 (here referred to as 'passive diffusion'), or through operating carbon-concentrating mechanisms (referred to as 'active transport'). The influx rate of passive diffusion of a nutrient can be quantified using Fick's Law as:

$$J = \frac{D(C_b - C_s)}{\delta} \quad \text{Eqn 1}$$

where J is the diffusive influx rate of nutrient solute from the bulk medium to the cell surface (mol m^{-2} s^{-1}), D is the diffusion coefficient of the solute (m^2 s^{-1}), δ is the thickness of the boundary layer (m) and C_b and C_s are the concentrations (mol m^{-3}) in the bulk medium and at the cell surface, respectively. Hence, considering only external diffusion, theory predicts that smaller cells should have higher volume-specific rates of CO_2 uptake because of a thinner diffusion boundary layer and a greater surface area-to-volume quotient than larger cells.

All cyanobacteria and most microalgal species possess active transport systems for movement of dissolved inorganic carbon (DIC) between the plasmalemma and Rubisco (Raven *et al.*, 2017). Specifically, CO_2-concentrating mechanisms (CCMs) use energy to elevate the steady-state CO_2 concentration at the active site of Rubisco (Giordano *et al.*, 2005). CCMs increase the affinity of carbon uptake and gross CO_2 fixation by the photosynthesis–photorespiration system by restricting energy-costly photorespiratory CO_2 loss (Raven *et al.*, 2014). However, the production and operation of CCMs generally increase the

energetic costs of carbon fixation compared to relying on diffusive CO_2 influx, especially at higher external CO_2 concentrations when there is less photorespiration (Tortell, 2000; Hopkinson *et al.*, 2011; Raven *et al.*, 2014). As a result, cells downregulate active transport at high concentrations of external CO_2, when diffusional CO_2 flux from the medium to Rubisco is sufficient to a maintain steady-state CO_2 concentration at the site of Rubisco to support photosynthesis (Giordano *et al.*, 2005; Raven *et al.*, 2017). Although it has been argued that very small cells might rely solely on diffusive CO_2 flux to Rubisco (Raven, 1998), even the smallest prokaryotic (e.g. *Prochlorococcus*; Hopkinson *et al.*, 2014) and eukaryotic species (e.g. *Micromonas pusilla*; Iglesias-Rodriguez *et al.*, 1998) use CCMs that increase their internal carbon pools.

Overall, there are contrasting predictions on the benefits of smaller and larger cells for the net carbon budget of a phytoplankton species. On the one hand, Fick's Law would predict smaller cells to have a greater CO_2 diffusive supply to the cell membrane (Raven, 1987; Raven & Kübler, 2002; Beardall *et al.*, 2009; Finkel *et al.*, 2010; Raven & Beardall, 2018), but on the other hand larger cells have greater scope to invest metabolic energy into active transport across the cell membrane by upregulating CCMs per unit area, provided that the plasmalemma of cells with a lower area : volume quotient has room for more CCM-related transporters (Raven, 1987; Tortell, 2000). Exposing phytoplankton communities to increased CO_2 concentrations affects the cell size distribution, implying cell size influences DIC assimilation, but the diversity of responses confounds simple expectations regarding which size will be favoured across a CO_2 gradient (Beardall *et al.*, 2009; Finkel *et al.*, 2010; Wu *et al.*, 2014; Sett *et al.*, 2018).

A major complication for understanding the role of cell size on phytoplankton carbon assimilation is that experimental tests rely heavily on among-species comparisons (e.g. Riebesell *et al.*, 1993; Burkhardt *et al.*, 1999; Tortell *et al.*, 2008; Wu *et al.*, 2014; Sett *et al.*, 2018). While an essential first step, comparisons across different species provide limited insights into the underlying causal effects, because many biotic and abiotic variables systematically covary with cell size or ambient CO_2 levels. For example, species with larger cells in the nano- to mesoplankton range also have a suite of other correlated traits, such as greater per-cell nutrient requirements (Edwards *et al.*, 2012), lower specific growth rate and hence longer generation time (Edwards *et al.*, 2015), higher nutrient storage potential (Shuter, 1978), and lower mass-specific energy use (Maranon, 2015). Moreover, environments with high ambient CO_2 usually have high inorganic nutrients (Christian *et al.*, 1997), lower temperatures (Lee *et al.*, 2000) and lower light penetration (Christian *et al.*, 1997; Lee *et al.*, 2000), as well as varying predictably across latitude/longitude and seasons (Friederich *et al.*, 2002). Hence, correlations with other biological and physical factors complicate our understanding of the physiological repercussions of cell size *per se* on phytoplankton carbon assimilation. An alternative approach to better assess causal relationships would be to manipulate the cell size of a species and assess the expression of other traits. However, within-species studies exploring the consequences of phytoplankton cell size remain very rare.

The aim of this study was to quantify the effects of cell size on microalgal carbon acquisition by comparing lineages of the same species that differ in mean cell sizes. Specifically, we used 400 generations (*c.* 3 yr) of artificial selection to evolve a 9.3-fold difference in cell volume between small-selected and large-selected lineages of the green alga *Dunaliella tertiolecta* – while controlling for other biotic and abiotic factors. In the past, we have used this model system to assess the effects of cell size on photosynthesis (Malerba *et al.*, 2018b,c), demographic rates (Malerba *et al.*, 2018a; Malerba & Marshall, 2019), thermal tolerance (Malerba & Marshall, 2020) and genome size (Malerba *et al.*, 2020). In this study, we first constructed photosynthesis vs dissolved inorganic carbon (P vs DIC) curves to estimate the performance of a cell across a resource gradient, specifically to determine the kinetics of DIC utilization as a measure of the activity of CCMs across cell sizes. Second, we used physical models to evaluate the diffusive supply to the cell surface and to calculate the total carbon demand relative to diffusive supply. Third, we obtained additional information about active carbon uptake by measuring the external carbonic anhydrase activity (CA_{ext}) and isotopic signature ($\delta^{13}C$) among cells of different sizes. Finally, we measured the overall effect of cell size on population-level fitness (i.e. maximum specific growth rate, maximum biovolume density). Following Fick's Law, our hypothesis is that increasing cell size would reduce the ability of a species to use passive diffusion to take up DIC from the medium. As a result, we would expect small-selected cells to be less carbon-limited and present superior performance for DIC uptake and growth than large-selected cells.

Materials and Methods

Study species

We sourced monoclonal cultures of the cosmopolitan, fast growing green alga *Dunaliella tertiolecta* (Butcher) from the Australian National Algae Culture Collection (ANACC; strain code CS-14). We grew all cultures in batch culture with autoclaved f/2 medium (without silica) prepared with 0.45 μm filtered seawater (Guillard, 1975) at 21 ± 2°C at a photon flux of *c.* 200 μmol photons m^{-2} s^{-1} with a 14 h : 10 h, day : night cycle.

Artificial selection for size

Details on the artificial selection protocols are given by Malerba *et al.* (2018c). Briefly, larger cells form a pellet at the bottom of test tubes at lower centrifugal forces compared to smaller cells, which instead remain in solution (i.e. differential centrifugation). On 25 April 2016, we inoculated 72 lineages from the same ancestral population of *D. tertiolecta* into aseptic plastic cell culture flasks (Corning, NY, USA; canted neck, nonpyrogenic, 75 cm^2 surface volume, vented cap). Since then, we have selected all lineages twice a week, each Monday and Thursday: 30 lineages were large-selected, 30 small-selected and 12 were the control.

We selected large cells by only retaining the biomass pellet after centrifuging at 38 ***g*** (600 rpm) for 3 min, whereas we selected for small cells by retaining only the supernatant after centrifuging at 68 ***g*** (800 rpm) for 4 min. We carried out each centrifugation routine twice for each selection round. As cells evolved in size, we adjusted the speed and duration of differential centrifugation to maintain an 80% dilution of the initial density. At the end of the selection process, we used one more centrifugation at 239 ***g*** (1500 rpm) for 4 min to resuspend all remaining cells into fresh media. Control cultures experienced identical conditions (including centrifugation) without size-selection. Lineages were not axenic, but we kept bacterial loads to low levels by resuspending pelleted cells in autoclaved medium twice a week and by handling samples using sterile materials under a laminar-flow cabinet (Gelman Sciences Australia, CF23S, NATA certified). Unless stated otherwise, all chemicals were of analytical grade and sourced from Sigma-Aldrich.

Experimental trials

All experiments took place between 367 and 403 generations of artificial selection (see Fig. 1 for evolutionary trajectories), with generation time estimated based on the ancestral strain (i.e. three generations in a week). To remove any environmental effects and nongenetic phenotypic differences from the size-selection protocols, before starting trials we exposed all cells to three generations (a week) of common garden conditions with no centrifugation (neutral conditioning).

Cell size, flagella length and population density

Following neutral conditioning, we estimated population density in 12 randomly selected lineages using manual cell counting, by loading 10 µl of Lugol-stained sample in a haemocytometer (Neubauer Improved, Bright-line double ruled; Pacific Lab). Then, we traced the 2D cross-sectional area and the length of the two flagella in individual cells using light microscopy at ×400 and Fiji 2.0 (Schindelin *et al.*, 2012), after staining around 200 cells per lineage with Lugol's iodine at 2%. We ensured that there was no detectable shrinkage associated with Lugol staining (see Malerba *et al.*, 2018c). We calculated cell volume (µm^3) assuming a prolate spheroid shape, as recommended for this species by Hillebrand *et al.* (1999):

$$\text{Cell volume} = \frac{\pi}{6} a b^2 \qquad \text{Eqn 2}$$

where a and b are the major and minor semi-axes (µm) of the fitted ellipse inside the cross-sectional area of the cell, respectively. Then, we calculated the surface area by rotating the area of the fitted ellipse along the major axis, as:

$$\text{Surface area} = \frac{\pi b}{2}\left(b + \frac{a^2}{\sqrt{a^2 - b^2}} \sin^{-1} \frac{\sqrt{a^2 - b^2}}{a}\right) \qquad \text{Eqn 3}$$

Carbon utilization

After 1 wk of neutral conditioning, we pooled together different lineages to make three replicate cultures of 100 ml for each of the three size-selection treatments (total of nine cultures; see Supporting Information Table S1 for the experimental design). To make each of those cultures, we used 10 ml of each of 10 lineages (for both large- and small-selected treatments) and 25 ml of each of four lines (for the control lineages). We resuspended cells in each flask into fresh medium in 1-l glass Erlenmeyer flasks. To maintain statistical independence among replicate flasks, cells from each lineage contributed to only one flask (see Table S1 for more details on replication).

For 1 wk before the experiment, we bubbled all cultures and medium with air to ensure equilibrium with ambient DIC. We also monitored the pH of cultures and fresh medium for 1 wk before experimental sampling, as a proxy to ensure the DIC system was close to air equilibrium (i.e. pH *c.* 7.9–8). For 5 d, we diluted the cultures each day by adding 50% of medium (semi-continuous cultures) and all experiments took place on the sixth day. Pilot assays revealed that biovolume was a better predictor of resource usage by our cultures than population density and we showed that blank-corrected optical density at 750 nm (OD_{750}) is a reasonable proxy for the total biovolume in a culture (Malerba *et al.*, 2018a,c). We therefore took all measurements after resuspending cells in fresh medium and standardizing to an intermediate biovolume density at an OD_{750} of 0.5 in a 1 cm pathlength cell – on average corresponding to 5415, 2530 and 1385 cells µl^{-1} for small-selected control, and large-selected lineages, respectively (determined by manual cell counting). We measured three carbon utilization parameters for each 1-l flask: DIC system parameters, photosynthesis vs DIC, and external carbonic anhydrase (CA_{ext}). Finally, we used physical models to calculate the demand and supply for CO_2 of a cell. We repeated all

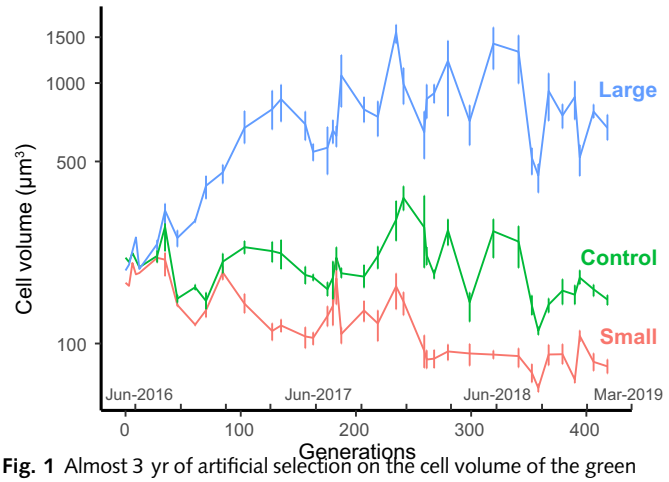

Fig. 1 Almost 3 yr of artificial selection on the cell volume of the green alga *Dunaliella tertiolecta*. Coloured lines track the mean size for each size-selected treatment (± 95% CI). All experimental trials occurred after between 367 and 403 generations of artificial selection, when the mean cell volume of large-selected lineages (976 µm^3) was 7.2 and 4.5 times larger than that of small-selected (135 µm^3) and control lineages (219 µm^3), respectively. Generation numbers are based on the growth rate of the ancestral strain (i.e. three generations in a week).

experiments for the carbon utilization parameters over three successive weeks, each week analysing a replicate for each size-selected treatment.

DIC system parameters We collected cells by filtration through a 0.45 μm membrane to analyse the inorganic carbon system parameters in the supernatant of each of the nine 1-l flasks, according to the procedures described by Smith-Harding *et al.* (2017) that were based on the methods of Weiss (1974), Dickson & Riley (1979) and Millero (2010). We processed all samples immediately to prevent re-equilibration with air and ensure measurements reflected the DIC system within the cultures at the time of harvesting. In short, we first measured the pH of the filtered supernatant using a sensION + PH31 meter (Hach, Loveland, CO, USA). Then, we measured the CO_2 released after injecting 2 ml of medium into 20 ml of 0.1 M HCl, using an infra-red gas analysis system (Li-840A CO_2/H_2O Gas Analyzer; Li-Cor, Lincoln, NE, USA). We used a freshly prepared calibration curve of known sodium bicarbonate concentrations to estimate the total DIC in the sample. Finally, we used the pH values and the total DIC to calculate the concentration of the components of the DIC system (CO_2, HCO_3^- and CO_3^{2-}) using CO2SYS software (Pierrot *et al.*, 2006).

Oxygen evolution vs DIC We determined the DIC affinity of cells in each of the nine 1-l flasks by measuring O_2 evolution at a range of DIC concentrations (P vs DIC curves) in a Clark-type O_2 electrode (Hansatech Oxygraph). We prepared DIC-free medium by acidification to pH *c.* 2 with 32% HCl and by bubbling with nitrogen (N_2) gas for at least 90 min. We centrifuged (239 ***g***, 1500 rpm, 4 min) and washed all cells three times in DIC-free medium buffered with 10 mM Tris-base (Sigma) and adjusted to pH 8.2 with freshly prepared saturated sodium hydroxide and then concentrated samples to a standardized biovolume density at an OD_{750} of 2.0 – on average corresponding to 43 570, 23 191 and 5710 cells μl^{-1} for small-selected, control and large-selected lineages, respectively (determined by manual cell counting). We placed each 2 ml sample in the O_2-electrode chamber, maintained at 21°C by a circulating water bath and we monitored O_2 evolution at a saturating photon flux of 300 μmol photons m^{-2} s^{-1}. We left samples in the chamber until they reached the DIC compensation point after consuming residual DIC in the medium. We then measured photosynthetic oxygen evolution after 10 sequential additions of sodium bicarbonate (5–2000 mM). For each time-series of oxygen evolution, we standardized values for biovolume density before fitting a Michaelis–Menten curve using GRAPHPAD PRISM 6.07 (GraphPad Software, La Jolla, CA, USA) to obtain the half-saturation constant for DIC ($k_{0.5}$DIC) and per-cell maximum rate of DIC-saturated photosynthesis (P_{max}). Assuming complete equilibrium of DIC in the O_2-electrode chamber, we calculated the half-saturation constants specific to CO_2 ($k_{0.5}CO_2$) by using pH, salinity and temperature as described above for the DIC system parameters. We calculated per-cell conductance (the initial slope of photosynthesis vs CO_2 concentration) as $\frac{1}{2}P_{max}/K_{0.5}CO_2$. Finally, we used simple linear models to analyse changes in P_{max}, $k_{0.5}CO_2$ and conductance as a function of mean cell volume (continuous predictor).

External carbonic anhydrase (CA_{ext}) CA_{ext} activity increases the speed of re-equilibration of inorganic C and hence the supply of CO_2 at the cell surface from HCO_3^-, the main DIC species diffusing to the cell surface from seawater (Young *et al.*, 2001; Giordano *et al.*, 2005). CA_{ext} is not involved directly in active transport through the membrane and also occurs in species lacking a CCM, such as the red marine macroalga *Membranoptera alata* (Giordano & Maberly, 1989; Maberly, 1990; Raven *et al.*, 2002, 2020). To quantify CA_{ext} activity in each of the nine 1-l flasks, we used an electrometric assay (Wilbur & Anderson, 1948; Miyachi *et al.*, 1983), as modified by Young *et al.* (2001). We washed cells three times in ice cold 50 mM Na_2HPO_4 buffer containing 22 g l^{-1} NaCl and standardized each sample in 15 ml at a final OD_{750} of 0.5. After placing each sample in a stirred sealed chamber cooled at 4°C using a circulating water bath, we measured the time required for the pH to drop by 1 unit (starting from *c.* 7.8) in both the buffer solution with cells and in the cell-free buffer, after injecting 2.3 ml of a CO_2-saturated 22 g l^{-1} NaCl solution to an equal volume of sample. We repeated the procedure at least six times for each sample and we calculated CA_{ext} in units of relative enzyme activity (REA), as:

$$\text{Relative enzyme activity (REA)} = 10 \times \left(\frac{T_{\text{control}}}{T_{\text{cells}}} - 1 \right) \qquad \text{Eqn 4}$$

where $T_{control}$ and T_{cells} are the average times (in seconds) for a 1 pH unit drop in control and cell samples, respectively. For the analysis, we fitted an exponential model of the form $\log_{10}CA = a + b \times \log_{10}\text{Cell volume}$; if the 95% confidence intervals of the size-scaling coefficient (b) did not include 1, the relationship was deemed to be nonlinear.

Demand and supply for CO_2 For the CO_2 demand of a cell, we used the highest level of carbon uptake measured at light- and DIC-saturated photosynthesis, which corresponds to the parameter P_{max} of the P vs DIC curve. For CO_2 supply to the cell surface, we used the approaches of Miller & Colman (1980), Riebesell *et al.* (1993), Wolf-Gladrow & Riebesell (1997) and Reinfelder (2011), as:

$$Q_D = 4\pi \text{RD} \left(1 + R\sqrt{\frac{\dot{K}}{D}} \right) \left([CO_2]_{\text{bulk}} - [CO_2]_{\text{surface}} \right) \qquad \text{Eqn 5}$$

where Q_D is the CO_2 diffusive supply to the cell surface (mol cell s^{-1}), R is the cell radius (cm), D is the diffusivity of CO_2 in water (cm^2 s^{-1}), $[CO_2]_{bulk}$ and $[CO_2]_{surface}$ are the bulk and cell-surface concentrations of CO_2 (mol l^{-1}), and $\dot{K}$ is a first-order rate constant for the rate of formation of CO_2 from the dehydration of HCO_3^-. Values for $\dot{K}$ at the appropriate salinity and temperature were estimated following Johnson (1982). Hence, the demand : supply ratio (D : S) of a cell becomes P_{max}/Q_D.

Similar to the analysis of CA_{ext}, we fitted an exponential model of the form $\log_{10}D:S = a + b \times \log_{10}$Cell volume and investigated the 95% confidence intervals around b.

Isotopic carbon signature

For $\delta^{13}C$, the default assumptions are that: there is no $^{13}C/^{12}C$ discrimination in transmembrane (plasmalemma, chloroplast membranes) transport of CO_2 or HCO_3^- and little discrimination in diffusion through aqueous solutions; CA (external and internal) activities are adequate to establish chemical and isotopic values of CO_2 and HCO_3^- in all compartments; and Rubisco has large discrimination when there is no diffusive limitation (Raven *et al.*, 2002). Values of $\delta^{13}C < -30‰$ indicate diffusive CO_2 flux from the medium to Rubisco, whereas values $> -10‰$ suggest active DIC influx through CCMs with no or little leakage of CO_2 back to the medium. Intermediate values suggest either diffusive flux of CO_2 from the medium to the Rubisco active site (with higher values indicating increased diffusion limitation) or the presence of a CCM (Raven *et al.*, 2002). In the presence of a CCM, and all else (e.g. diffusion boundary layer thickness, carbon fixation rates, growth rates) being equal, an increase in $\delta^{13}C$ is consistent with less CO_2 leakage and hence a greater ability to concentrate DIC against a free energy gradient (Fogel *et al.*, 1992; Fielding *et al.*, 1998; Raven *et al.*, 2002).

We used standard methods (Fry, 2006) to quantify the isotopic carbon signature $\delta^{13}C$ from five algal lineages for each size-selection treatment (total of 15 samples; see Table S1 for the experimental design). To ensure nonlimiting resources and DIC near air equilibrium, we used aerated batch cultures and sampled the biomass during the exponential phase. For each lineage, we filtered a known concentration of cell biovolume (estimated using OD_{750}) onto preweighed paper filters (Whatman GF/C, diameter 47 mm). We sent all samples to the Water Studies Centre (Monash University) to quantify the isotopic carbon $\delta^{13}C$ signature from the fraction of ^{13}C and ^{12}C between sample and standard, using the ANCA GSL2 elemental analyser interfaced to a Hydra 20–22 continuous-flow isotope ratio mass spectrometer (Sercon Ltd, Crewe, UK), as:

$$\delta^{13}C = \left(\frac{\left(\frac{^{13}C}{^{12}C}\right)_{sample}}{\left(\frac{^{13}C}{^{12}C}\right)_{standard}} - 1 \right) \times 1000‰ \quad \text{Eqn 6}$$

The QA/QC procedure used three internal standards (sucrose, gelatin and bream). Standards corrected for variation as results of peak size linearity and instrumental drift with a typical reproducibility of ± 0.2‰. Based on internal standards, the accuracy of the data was within ± 0.2‰. We calibrated all the internal standards against internationally recognized reference materials which include USGS 40, USGS 41 and IAEA C-6 (the certified values can be obtained from the website of the Water Studies Centre). We used a simple linear regression to analyse the effect of mean cell volume on $\delta^{13}C$. Values for $\delta^{13}C$ are not corrected for source DIC, but we assumed source values are identical across treatments as we used the same aeration procedure for all samples.

Growth curves

We estimated the maximum growth rate and the maximum biovolume density of 12 randomly selected lineages for each size-selection treatment (total of 36 samples). We used methods described by Malerba *et al.* (2018a) and Malerba & Marshall (2019). Briefly, we loaded each lineage into three independent 96-well plates (Corning polystyrene, flat bottom, with lid, sterile, nontreated; Sigma-Aldrich), randomizing the position within the plate, after resuspending cells into 250 µl of standard fresh f/2 medium and standardizing initial populations to the same blank-corrected optical density (at 750 nm). We used light-saturated conditions (*c.* 300 µmol m^{-2} s^{-1}) at a 14h : 10 h, day : night cycle to grow all plates and we monitored the blank-corrected optical density (750 nm) for 5 d (at the same time into the photoperiod) using a SPECTROstar Nano plate reader (BMG Labtech, Offenburg, Germany). This indirect way to measure biomass production allowed for more frequent (nondestructive) monitoring compared to direct methods (e.g. flow cytometry). A pilot study showed that evaporation in the wells was low (*c.* 1% per day) and was therefore ignored in the analysis.

For statistical analysis of the growth curves, we fitted three nonlinear logistic-type models to describe the change in total biovolume production over time in each well: a logistic sinusoidal curve with lower asymptote forced to 0, a more general logistic curve with a nonzero asymptote, and a 'Gompertz with mortality' sinusoidal model with a population decline after reaching a maximum biovolume density (for a graphical explanation and more details on the models, see Figs S3 and S4 in Malerba *et al.*, 2018a). We removed those models that failed to converge. From the best-fitting growth model following Akaike's Information Criterion (Burnham & Anderson, 2004), we extracted the maximum predicted value of total biovolume (K; units of µm^3 µl^{-1}), which represents the total biomass reached at the end of the time-series. From the first derivative of the best-fitting growth model, we extracted the maximum intrinsic growth rate (r; units of d^{-1}), which represents the maximum observed growth rate of the population. Finally, we used two separate linear models to analyse r and K as a function of the size-selection treatment (categorical variable).

Transmission electron microscopy

We adopted the methods developed by Clayton (1986) to image cells from five randomly selected lineages for each size-selected treatment. First, we spun down (300 ***g***, 8 min) and resuspended cells in 15 ml of sterile filtered seawater with 1% of glutaraldehyde and 1% osmium tetroxide at room temperature for 2 h. After rinsing in sterile filtered seawater three times, we dehydrated cells to 100% ethanol in incremental steps of 10% for 10 min each (leaving at 70% ethanol overnight). Infiltration in 10% firm grade Spurr's resin started after cells were placed in 100% propylene oxide for 30 min. Spurr's resin was added at

incremental steps from 20% to 100%, leaving samples overnight between each step. We embedded and polymerized samples overnight at 60°C, sectioning at 120–150 μm using formvar-coated slot grids. Finally, we viewed cells in a Jeol JEM-1400Plus transmission electron microscope. We identified intracellular characteristics by comparing with other studies on the same genus (Bérubé *et al.*, 1999; Bidle & Falkowski, 2004; Jimenez *et al.*, 2009; Heakal *et al.*, 2010).

Results

External cell morphology

Throughout the 400 generations of artificial selection, the mean cell volume increased by 0.47% per generation in large-selected lineages ($F_{1,48} = 126$, $P < 0.001$), and decreased by 0.21% in small-selected lineages ($F_{1,48} = 122.8$, $P < 0.001$). Control lineages showed fluctuations in cell size, but without any systematic trend over time ($F_{1,42} = 0.299$, $P = 0.59$; Fig. 1).

Experiments took place between 367 and 403 generations of artificial selection, when the mean cell volume of large-selected lineages (752 μm^3) was 9.3 and 5.3 times larger than that of small-selected (80 μm^3) and control lineages (141 μm^3), respectively (Fig. 1). Cell surface area ranged from 90 to 370 μm^2 among lineages and the surface area to volume quotient decreased by 2.2-fold from small- to large-selected cultures. Furthermore, there was a 19% increase in the mean length of the flagella, from 11.5 μm in small-selected cells, to 12.1 μm in control cells and to 13.7 μm in large-selected cells, as measured from 1851 cells across 38 lineages using optical microscopy ($\chi^2 = 143.97$, df = 2, $P < 0.001$; data not shown).

Cell ultrastructure

Although our transmission electron micrographs cannot offer a reliable quantification of properties, a qualitative assessment suggests that large-selected cells per volume may contain more starch, chloroplasts and mitochondria compared to small-selected and control cells (Fig. 2). Other characteristics appeared less affected, such as the thickness of the glycocalyx-type cell covering (Fig. 2; all original transmission electron micrographs are available in the data repository).

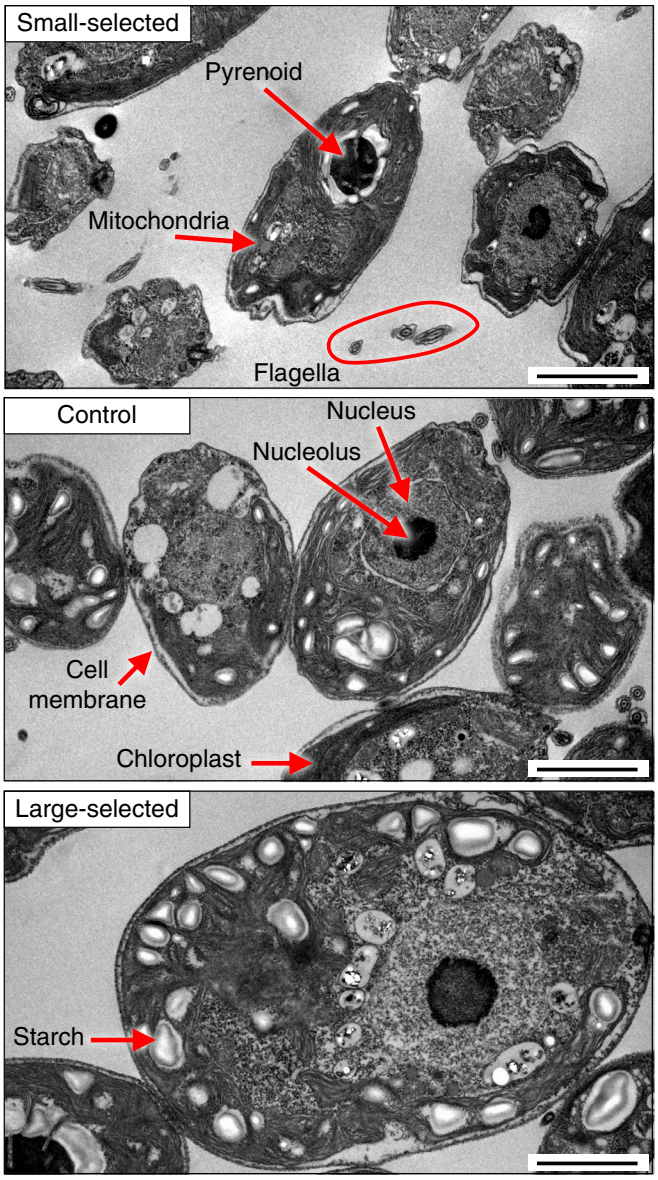

Fig. 2 Morphological characteristics of *Dunaliella tertiolecta* from the three artificial selection treatments in transmission electron micrographs at ×10 000. These images are for illustrative purposes only and do not offer a reliable quantification of absolute or volume-specific properties. Bars, 2 μm.

Photosynthesis vs DIC relationship

All parameters of the *P* vs DIC curves changed with the mean cell volume of the culture. Specifically, the half-saturation constant ($k_{0.5}CO_2$) decreased with increasing cell size (Fig. 3a), while maximum photosynthesis (P_{max}) and conductance increased with cell size (Fig. 3b,c). Importantly, both P_{max} and conductance increased proportionally to cell volume (see overlapping continuous and dashed lines in Fig. 3b,c), indicating that a doubling of cell volume corresponded to a doubling of P_{max} and conductance.

Trials in experimental run 1 showed higher-than-air equilibrium CO_2 concentrations in all cultures (40.3 ± 8.4 μM) compared to the next two runs (18.6 ± 9.6 μM). We therefore decided to retain only the data from runs 2 and 3 in the analyses. Importantly, all qualitative trends remained identical across all 3 wk of experiments (see Fig S1 for comparison). Also, there was no systematic trend between CO_2 concentrations and size-selection treatment (i.e. the residuals were random among replicates), so we can exclude any effects of CO_2 variations on the overall conclusions.

External carbonic anhydrase (CA_{ext}) activity

CA_{ext} activity, measured as REA, increased as cells evolved to larger sizes (Fig. 4). The relationship revealed an isometric size-

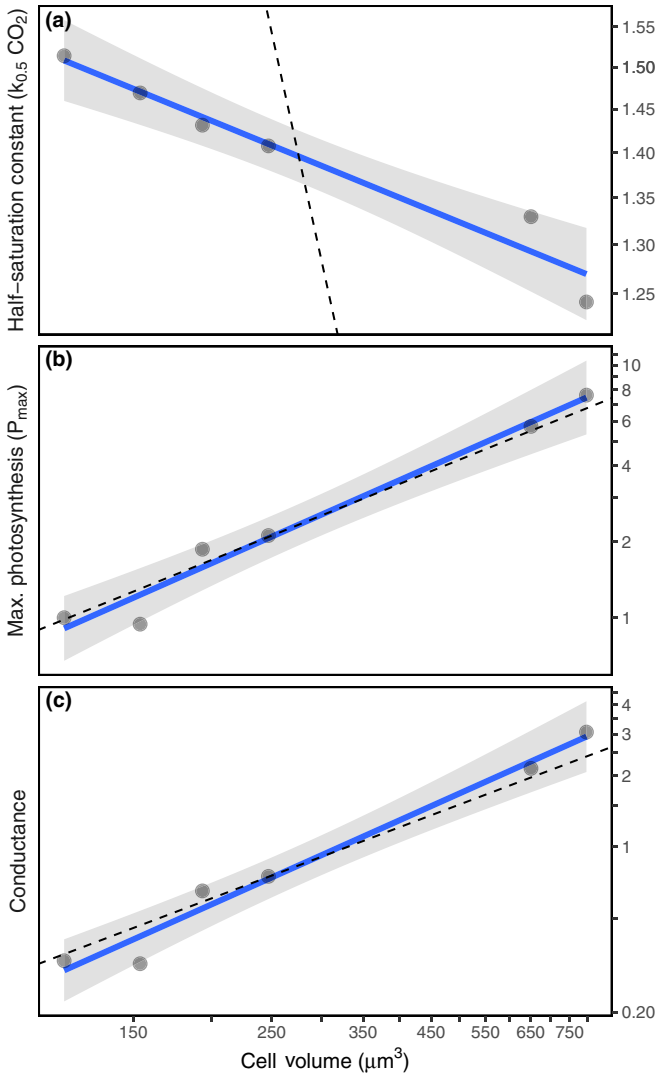

Fig. 3 Effects of cell volume of *Dunaliella tertiolecta* on the (a) half-saturation constant for CO_2 (units: μmol CO_2 l^{-1}), (b) maximum photosynthetic rates (units: 10^{-6} nmol CO_2 min^{-1} per cell) and (c) conductance (units: 10^{-6} nmol CO_2 min^{-1} per cell (μmol CO_2 $l^{-1})^{-1}$). Each dot indicates an independent culture with a different mean cell size. Continuous lines (± 95% CI) indicate statistically significant least-square linear regressions ($k_{0.5}CO_2$: $R^2 = 0.95$, $F_{1,4} = 73.17$, $P = 0.001$; P_{max}: $R^2 = 0.97$, $F_{1,4} = 133.3$, $P < 0.001$; conductance: $R^2 = 0.97$, $F_{1,4} = 148.7$, $P < 0.001$). Dashed lines indicate isometric slopes (with the intercepts estimated from the data). Hence, a dashed line overlapping a linear regression indicates a proportional change between the response variable and cell volume (i.e. doubling *x* corresponds to doubling *y*). Data collected during the first experimental run were excluded from the main analyses, but are presented for comparative purposes in Supporting Information Fig. S1.

scaling slope of 1.05 (95% confidence interval (CI): 0.41–1.69), which indicates a proportional increase between CA_{ext} and the volume of the cell (see close match between continuous and dashed lines in Fig. 4). Given that the surface area to cell volume quotient decreases with cell volume (i.e. size-scaling of 0.6; see dotted line in Fig. 4), this means that the concentration of CA_{ext} on the cell surface increased with increasing cell volume –

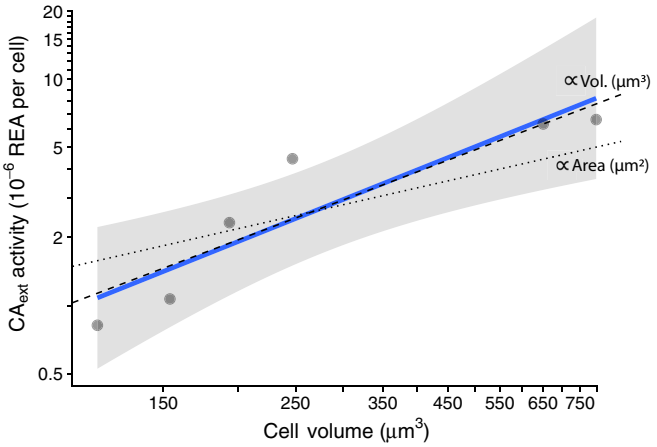

Fig. 4 Scaling relationship between cell surface area and external carbonic anhydrase activity (CA_{ext}) in *Dunaliella tertiolecta*, expressed in units of relative enzyme activity (REA) per cell. Continuous line (± 95% CI) indicates the fit of the model ($\log_{10}CA = a + b \times \log_{10}$Cell volume; $R^2 = 0.53$, $F_{1,4} = 20.85$, $P = 0.01$). The estimated slope was 1.05 (95% CI: 0.41–1.69). Each dot indicates an independent culture with a different mean cell size. The dashed line indicates a proportionality with cell volume (slope of 1) and dotted line indicates proportionality with surface area (slope of 0.6), with both intercepts estimated from the data.

although this increase was statistically significant only at 88% confidence (see overlap between dotted line and grey shading in Fig. 4). Specifically, the mean CA_{ext} per unit area increased nearly 3-fold from smaller (7.5×10^{-9} REA μm^{-2}) to larger cells (18.7×10^{-9} REA μm^{-2}).

Ratio of demand to supply (D : S) for CO_2

The ratio of CO_2 demand (i.e. P_{max}) to diffusive supply (i.e. Q_D) scaled with cell volume at an exponent close to three quarters (0.76; Fig. 5). Both $k_{0.5}CO_2$ and CA_{ext} activity changed linearly with D : S ratio: $k_{0.5}CO_2$ decreased with increasing D : S (Fig. 6a), whereas CA_{ext} activity increased with increasing D : S (Fig. 6b).

Isotopic signature of $\delta^{13}C$

Algal biomass showed a positive linear relationship between $\delta^{13}C$ and cell volume (Fig. 7). Specifically, $\delta^{13}C$ increased (became less negative) by almost 3‰ (from −25.29‰ to −22.44‰) as cells increased in volume from 100 to 600 μm^3 (Fig. 7).

Growth rates

Populations of large-selected cells recorded higher maximum specific growth rates and reached higher maximum biovolume densities than populations of small-selected cells (Fig. 8). Specifically, a 6.5-fold increase in cell volume corresponded to a 2.4-fold increase in maximum specific growth rate (Fig. 8a) and to a 2.1-fold increase in maximum biovolume density (Fig. 8b). Importantly, the effect of cell size on maximum growth rates was nonlinear, with intermediate (control) cells recording maximum growth rates higher than small-selected cells but similar to large-selected cells (see Fig. 8a).

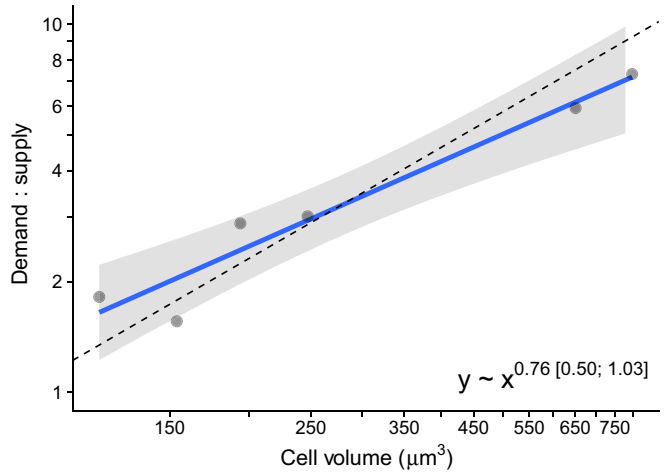

Fig. 5 The ratio of demand to diffusive supply of CO_2 as a function of cell volume in *Dunaliella tertiolecta*. Demand was quantified as the maximum rate of light- and DIC-saturated photosynthesis (i.e. P_{max} in Fig. 3a), whereas CO_2 diffusive supply to the cell surface (i.e. Q_D) was estimated using Eqn 3. Each dot indicates an independent culture with a different mean cell size. The continuous line (± 95% CI) indicates the fit of the model ($\log_{10}D : S = a + b \times \log_{10}$Cell volume; $R^2 = 0.94$, $F_{1,4} = 64.21$, $P = 0.001$). The dashed line indicates a rate of change that is proportional to cell volume (i.e. slope = 1), with the intercept (a) estimated from the data. The size-scaling slope (b) is reported on the plot (± 95% CI).

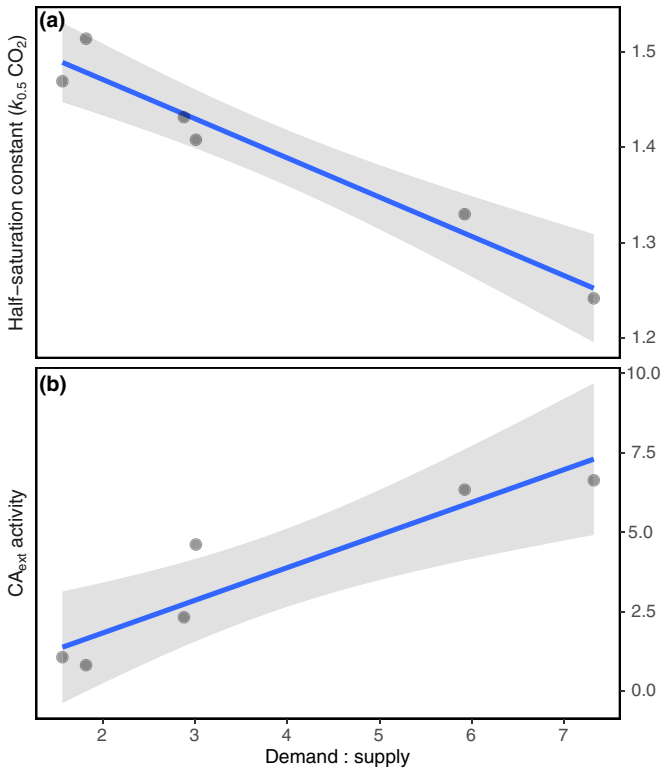

Fig. 6 Effects of demand-to-supply ratio for CO_2 on (a) half saturation constant ($k_{0.5}CO_2$; units of µmol l^{-1}) and (b) activity (CA_{ext}; units of relative enzyme activity) in *Dunaliella tertiolecta*. Each dot indicates an independent culture with a different mean cell size. Continuous lines (±95% CI) indicate the fits of least-square linear regressions ($k_{0.5}CO_2$: $R^2 = 0.95$, $F_{1,4} = 69.93$, $P = 0.001$; CA_{ext} activity: $R^2 = 0.86$, $F_{1,4} = 24.7$, $P = 0.008$).

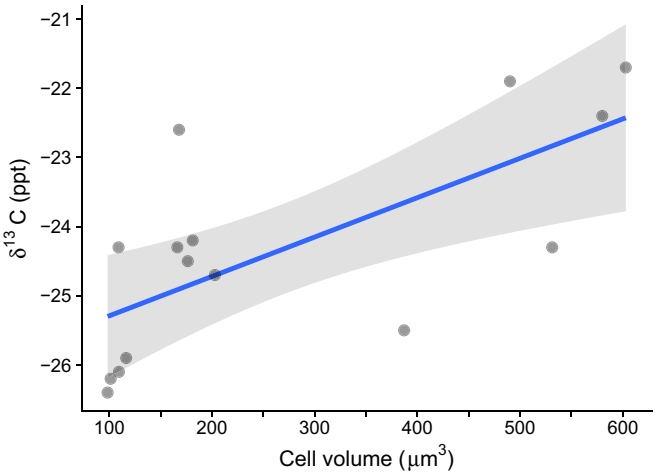

Fig. 7 Effect of cell volume of *Dunaliella tertiolecta* on the isotopic signature of $\delta^{13}C$ (units: ppt). Each dot indicates an independent culture with a different mean cell size. The continuous line (±95% CI) indicates statistically significant least-square linear regression ($R^2 = 0.48$, $F_{1,13} = 12.12$, $P = 0.004$).

Discussion

The size of phytoplankton cells influences the flux of DIC from the medium to inside the plasmalemma. As predicted from Fick's Law, larger cells would be expected to have a lower potential for DIC supply from passive diffusion and a higher ratio of DIC demand to diffusive supply, which – all else being equal – would suggest a greater degree of carbon limitation with increasing cell size. In our system, however, large-selected lineages performed better than small-selected ones, with faster growth rates and higher maximum biovolume densities, both here and in previous studies (Malerba & Marshall, 2019). Moreover, we found non-linear effects of cell size on maximum growth rate, with control and large-selected lineages recording similar values, although both exceed that of small-selected cells. This finding is also consistent with previous results and may indicate complex genetic effects of size-selection on cell growth (see Malerba *et al.*, 2018a for more details). Importantly, we found that the half-saturation constant ($k_{0.5}CO_2$) decreased with cell size while the external carbonic anhydrase activity (CA_{ext}) and isotopic signature ($\delta^{13}C$) increased with cell size, all of which indicate greater CCM expression as cells evolved to larger sizes. This increase in $\delta^{13}C$ with cell size is consistent with a reduction in CO_2 leakage from the accumulated DIC pool back to the medium, meaning larger cells are more efficient at using CCMs to transport carbon than smaller cells (Raven *et al.*, 2002).

Values of $k_{0.5}CO_2$ can provide information on the occurrence of CCMs in a culture (Raven *et al.*, 2002). The range of $k_{0.5}CO_2$ in our lineages (from 1.2 to 1.5 µM) is comparable with previous work on *D. tertiolecta* (see Table 1 in Raven, 2009). However, all our cultures showed much greater affinity (*c.* 20 times lower $k_{0.5}CO_2$) than the affinity of isolated Rubisco from pyrenoid-containing green algae (*c.* 35 µM; Iñiguez *et al.*, 2020). Given the small excess of CO_2-saturated Rubisco catalytic capacity in *Dunaliella* spp. (Giordano & Bowes, 1997; Flynn & Raven,

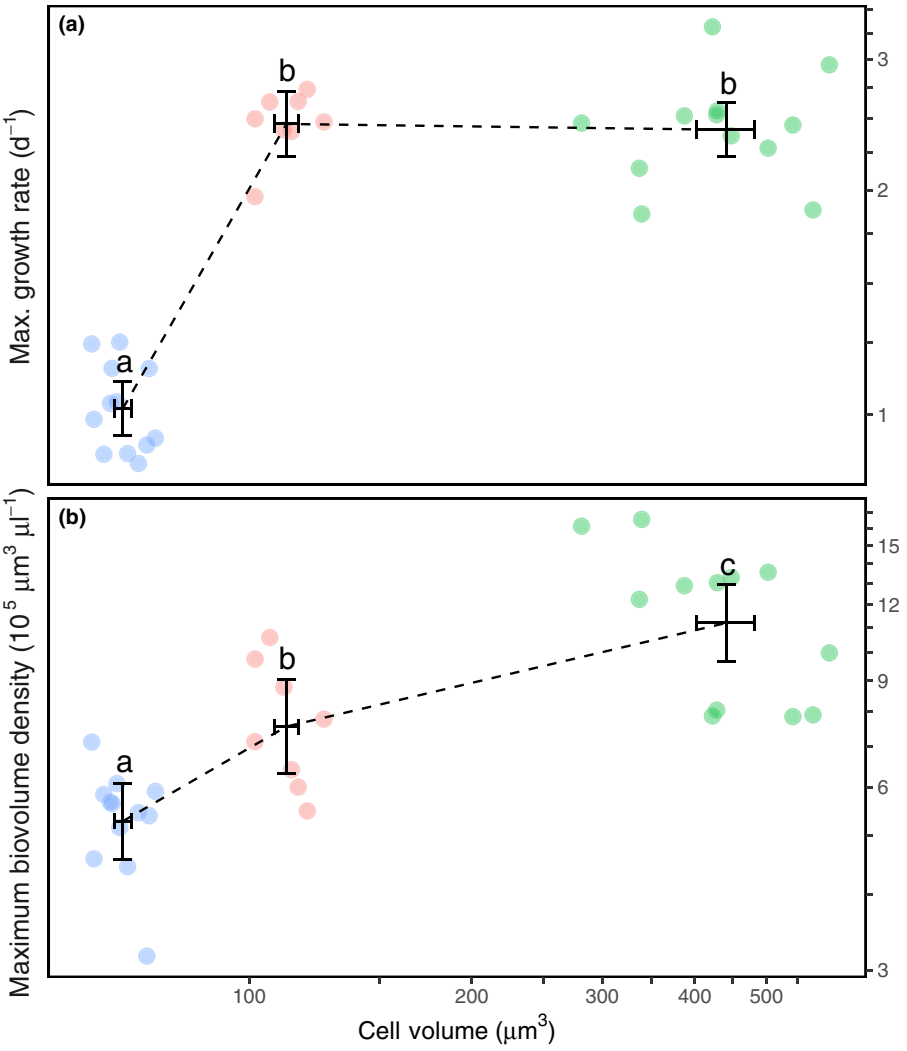

Fig. 8 Effects of cell volume of *Dunaliella tertiolecta* on population-level demographic parameters of (a) maximum specific growth rate and (b) maximum biovolume density. Each dot represents an independent lineage (total of 35 samples) and the colour represents its size-selection treatment (i.e. blue points are small-selected, red points are control and yellow points are large-selected lineages). Error bars indicate means (± 95% CI) for each treatment and lower case letters represent Tukey's *post-hoc* groupings (maximum growth rate: $F_{2,29} = 143.3$, $P < 0.001$; maximum biovolume density: $F_{2,29} = 28.228$, $P < 0.001$).

2017), the most likely explanation for the greater affinity in our lineages is the presence of a CCM driving DIC uptake and, hence, no role for diffusive CO_2 flux from the medium to Rubisco (Aizawa & Miyachi, 1984; Aizawa *et al.*, 1985; Burns & Beardall, 1987; Amoroso *et al.*, 1998; Young *et al.*, 2001). The absence of diffusion in *D. tertiolecta* in air-equilibrated seawater is because synthesizing enough Rubisco (> 10-fold increase) would require exorbitant investments in energy and nutrients, making diffusive CO_2 flux more costly than running and maintaining CCMs (Raven *et al.*, 2014).

Effects of cell size on DIC uptake mechanisms

Theory predicts that larger cells require a greater DIC influx from CCMs per unit surface area to compensate for their limited potential for diffusive flux compared to smaller cells (Raven, 1987; Raven & Kübler, 2002; Beardall *et al.*, 2009; Finkel *et al.*, 2010; Raven & Beardall, 2018). Our results are consistent with these predictions, with CA_{ext} and affinity for inorganic carbon (shown as lower $k_{0.5}CO_2$) increasing with cell volume. Importantly, given that CA_{ext} activity scaled proportionally to cell volume (i.e. size-scaling exponent close to 1) and that the surface-to-volume quotient decreases with increasing cell volume, it follows that the density of CA_{ext} per unit surface area must increase as the D : S ratio decreased, thus stimulating the supply of CO_2 in larger cells. Moreover, size-evolved cells sampled from multiple generations showed a constant proportionality between cell volume and cell carbon mass (see Fig. 3 in Malerba *et al.*, 2018b), which means that standardizing CA_{ext} for cell carbon mass or cell volume would yield the same qualitative results. A similar increase in CA_{ext} during carbon limitation is consistent with studies on the diatoms *Phaeodactylum tricornutum* (Iglesias-Rodriguez & Merrett, 1997), *Thalassiosira pseudonana* (Hopkinson *et al.*, 2013) and *Chaetoceros muelleri* (Smith-Harding *et al.*, 2017), and the coccolithophore *Emiliania huxleyi* (Nimer *et al.*, 1994). Furthermore, field studies on the dinoflagellate *Peridinium gatunense* have shown that cells respond to carbon limitation during an algal bloom by increasing CA_{ext} (Berman-Frank *et al.*, 1994). While our data are consistent with upregulation of CCMs with increasing cell size to improve DIC acquisition – as predicted by theory – further studies are needed to clarify the relative contribution of CO_2 and HCO_3^- to the DIC influx of size-evolved lineages.

It is worth noting that an increase in $\delta^{13}C$ (i.e. less negative values) is an indirect proxy typically interpreted as an upregulation of CCMs in microalgal cells (Fielding *et al.*, 1998), but other interpretations are possible. The process of transporting DIC against an energy gradient in a CCM causes an increase in the $\delta^{13}C$ of organic matter compared to CO_2 diffusing from the medium to Rubisco (Fogel *et al.*, 1992; Raven *et al.*, 2002). However, in theory, a decrease in $\delta^{13}C$ could also occur without changes in CCMs and only from a larger cell increasing carbon limitation, in particular from a thicker boundary layer or a thicker cell wall (Raven *et al.*, 2002, 2019). In our case, large-selected lineages grew faster and showed higher P_{max} than small-selected lineages, which is inconsistent with larger cells being more carbon-limited. Also, *D. tertiolecta* lacks a typical cell wall (Borowitzka, 2018) and measurements from transmission electron microscopy of the glycocalyx-type cell covering (Fig. 2) showed a comparable thickness of 0.0377 μm (±0.0018 SE) across cells of all sizes, which makes it is unlikely that 'cell wall' thickness has any influence on $\delta^{13}C$. Finally, the higher $\delta^{13}C$ in large-selected cells coincided with an increase in CA_{ext} and a decrease in $k_{0.5}CO_2$, which are diagnostic features of greater CCM activity among many microalgal species (Elzenga *et al.*, 2000; Beardall & Giordano, 2002; Giordano *et al.*, 2005; Young & Beardall, 2005). Hence, the available evidence indicates that the positive relationship between $\delta^{13}C$ and cell size in this species is a consequence of a greater expression of CCMs as cells evolved to larger volumes. However, the weak correlation between $\delta^{13}C$ and cell size suggests that multiple traits (e.g. growth rate, thickness of the boundary layer, leakage of DIC, carbon fixation) are influencing the isotopic signature of a lineage.

Implications for phytoplankton biogeography

The systematic upregulation of CCMs with increasing cell size shown here could be an important mechanism influencing biogeographical patterns among phytoplankton species. Classic theories predict that smaller cells are superior competitors for inorganic nutrients (including inorganic carbon) because of a more efficient diffusive flux arising from their greater surface to volume quotient and a smaller boundary layer (Grover, 1989; Aksnes & Egge, 1991; Raven, 1998). However, our results showed that active uptake is (at least) as important as passive (diffusive) uptake into the cell, which means that biogeographical patterns should be considered in light of both ambient nutrient availabilities, as well as the metabolic energy needed to operate CCMs. If the effects of cell size shown here are consistent across other species, we would predict that mass-specific energetic costs of carbon fixation are higher for larger cells than for smaller cells, because of a greater reliance on CCMs over passive diffusion. Hence, we would expect context-dependent costs and benefits of cell size: on the one hand, larger cells are favoured in high-light environments because of their greater energetic investments into active uptake of resources across the cell membrane. On the other, smaller cells can maintain growth in low-light environments, because of their more advantageous surface to volume quotient, their lower self-shading and their greater ability to meet their carbon budgets with less energy investments. Data from *D. tertiolecta* are consistent with this prediction: previous work has shown that large-selected lineages are superior competitors under high light and high nutrients, but small-selected lineages perform better under resource-limited regimes (Malerba *et al.*, 2018b,c). For other species, less is known, but there is some support for a production–efficiency trade-off between nutrient and light utilization among phytoplankton species, where an inferior competitor for a limiting nutrient under high light can gain a competitive advantage under low light (Huisman & Weissing, 1995; Litchman *et al.*, 2004; Yoshiyama *et al.*, 2009; Burson *et al.*, 2018). A useful next step would be to explicitly account for the role of active and passive uptake in determining competitive outcomes among species of different sizes across a light gradient. Specifically, we would predict that species with greater CCM expression would have a competitive advantage, but only under high light.

Macro-evolutionary patterns and size-scaling exponents

If the DIC uptake of a cell is limited by diffusion, theory predicts that rates of nutrient uptake should be proportional to the surface area (Beardall *et al.*, 2009). This implies that the carbon uptake rate of a cell should scale with its volume at an exponent from 0.66 (assuming cells retain a spherical shape) to *c.* 0.75 (assuming larger cells become more prolate spheroid; Niklas & Cobb, 2017). However, DIC uptake traits usually scale at a higher exponent, between 0.75 and > 1 (DeLong *et al.*, 2010; Lopez-Sandoval *et al.*, 2014; Maranon, 2015) and our study suggests a potential explanation. If cells increase their CCM expression and reduce their CO_2 leakage as they increase in size – as shown for this species – then it is possible under resource-replete conditions that the uptake rate of a cell can increase faster than its surface area and generate size-scaling exponents > 0.66. Consistent with this explanation, there is some evidence that CCM expression increases with the mean cell volume of the phytoplankton community (Francois *et al.*, 1993; Popp *et al.*, 1998). For example, there is some evidence that larger diatoms with a thicker boundary layer are more reliant on active carbon transport than smaller diatoms (Korb *et al.*, 1996). A more definitive test would be to verify a positive relationship among cell size, carbon uptake and CCM expression in a broad range of phytoplankton species.

Conclusions

Evolving cells of *D. tertiolecta* to larger sizes led to an upregulation of CCMs that improved the DIC uptake of this species, with higher CA_{ext}, higher $\delta^{13}C$ and higher CO_2 affinity. Large-selected cells also recorded faster growth and reached higher maximum biovolume densities than small-selected cells. Future marine ecosystems are likely to select for smaller phytoplankton cells through higher temperatures (Atkinson *et al.*, 2003; Gardner *et al.*, 2011). If the same relationships found here between cell size and carbon assimilation apply to other species, we may expect less carbon fixation from phytoplankton communities. Clearly, we need future studies to verify the generality of our

conclusions. For example, our experiments only used saturating light conditions and we cannot assume a similar response at lower light. For now, however, this study clearly shows that evolutionary shifts in cell size can alter the capacity and the efficiency of DIC uptake systems and affect the fitness of a phytoplankton species.

Acknowledgements

We thank Lucy Chapman, Belinda Comerford, Dr Tamsyne Smith-Harding, Dr Thomas Lines and Dr Yussi Palacios Delgado for their help with laboratory procedures. We also thank the Monash Centre for Electron Microscopy for their help with cell imaging, in particular Dr Georg Ramm, Dr Simon Crawford and Dr Joan Clark. We are grateful to the Water Studies Centre at Monash University for their help with measuring isotopic signatures, especially Prof. Perran Cook and Dr Wei Wen Wong. We would like to express our gratitude to Lesley Wiadrowski, Stewart Crowley and John Arvanitakis for logistical support at Monash University. Finally, we are particularly grateful to the Australian Research Council for financial support. The University of Dundee is a registered Scottish charity (no. 015096).

Author contributions

MEM, DJM and JB contributed to designing the study. MMP and MEM conducted the experiment. MEM, DJM and JB carried out statistical analyses. JB and MEM wrote the initial draft of the manuscript. DJM, JAR and MMP contributed substantially to interpreting the results, writing subsequent drafts and gave final approval for publication.

ORCID

John Beardall https://orcid.org/0000-0001-7684-446X
Martino E. Malerba https://orcid.org/0000-0002-7480-4779
Dustin J. Marshall https://orcid.org/0000-0001-6651-6219
Maria M. Palacios https://orcid.org/0000-0002-5450-674X
John A. Raven https://orcid.org/0000-0002-2789-3297

Data availability

All data generated during this study are available in a public internet repository in Mendeley data (http://dx.doi.org/10.17632/zbk84km29d.1). Also contained in the repository are the original photographs from optical microscopy and transmission electron microscopy of the size-evolved cells.

References

Aizawa K, Miyachi S. 1984. Carbonic anhydrase located on cell surface increases the affinity for inorganic carbon in photosynthesis of *Dunaliella tertiolecta*. *FEBS Letters* **173**: 41–44.

Aizawa K, Nakamura Y, Miyachi S. 1985. Variation of phosphoenolpyruvate carboxylase activity in *Dunaliella* associated with changes in atmospheric CO_2 concentration. *Plant and Cell Physiology* **26**: 1199–1203.

Aksnes DL, Egge JK. 1991. A theoretical model for nutrient uptake in phytoplankton. *Marine Ecology Progress Series* **70**: 65–72.

Amoroso O, Sültemeyer D, Thyssen C, Fock HP. 1998. Uptake of HCO_3^- and CO_2 in cells and chloroplasst of *Chlamydomonas reinhardtii* and *Dunaliella tertiolecta*. *Plant Physiology* **119**: 81–88.

Atkinson D, Ciotti BJ, Montagnes DJS. 2003. Protists decrease in size linearly with temperature: ca. 2.5% C−1. *Proceedings of the Royal Society of London B: Biological Sciences* **270**: 2605–2611.

Beardall J, Allen D, Bragg J, Finkel ZV, Flynn KJ, Quigg A, Rees TAV, Richardson A, Raven JA. 2009. Allometry and stoichiometry of unicellular, colonial and multicellular phytoplankton. *New Phytologist* **181**: 295–309.

Beardall J, Giordano M. 2002. Ecological implications of microalgal and cyanobacterial CO_2 concentrating mechanisms, and their regulation. *Functional Plant Biology* **29**: 335–347.

Berman-Frank I, Zohary T, Erez J, Dubinsky Z. 1994. CO_2 availability, carbonic anhydrase, and the annual dinoflagellate bloom in Lake Kinneret. *Limnology and Oceanography* **39**: 1822–1834.

Bérubé K, Dodge J, Ford T. 1999. Effects of chronic salt stress on the ultrastructure of *Dunaliella bioculata* (Chlorophyta, Volvocales): mechanisms of response and recovery. *European Journal of Phycology* **34**: 117–123.

Bidle KD, Falkowski PG. 2004. Cell death in planktonic, photosynthetic microorganisms. *Nature Review Microbiology* **2**: 643–655.

Borowitzka MA. 2018. Biology of Microalgae. 6.8.3 Dunaliella (Chlorophyta, Chlorophyceae, Dunaliellaceae). In: Levine I, Fleurence J, eds. *Microalgae in health and disease prevention*. London, UK: Elsevier, 23–72.

Burkhardt S, Zondervan I, Riebesell U. 1999. Effect of CO_2 concentration on C: N: P ratio in marine phytoplankton: a species comparison. *Limnology and Oceanography* **44**: 683–690.

Burnham KP, Anderson DR. 2004. Multimodel inference - understanding AIC and BIC in model selection. *Sociological Methods & Research* **33**: 261–304.

Burns BD, Beardall J. 1987. Utilization of inorganic carbon by marine microalgae. *Journal of Experimental Marine Biology and Ecology* **107**: 75–86.

Burson A, Stomp M, Greenwell E, Grosse J, Huisman J. 2018. Competition for nutrients and light: testing advances in resource competition with a natural phytoplankton community. *Ecology* **99**: 1108–1118.

Christian JR, Lewis MR, Karl DM. 1997. Vertical fluxes of carbon, nitrogen, and phosphorus in the North Pacific Subtropical Gyre near Hawaii. *Journal of Geophysical Research: Oceans* **102**(C7): 15667–15677.

Clayton MN. 1986. Culture studies on the life history of *Scytothamnus australis* and *Scytothamnus fasciculatus* (Phaeophyta) with electron microscope observations on sporogenesis and gametogenesis. *British Phycological Journal* **21**: 371–386.

DeLong JP, Okie JG, Moses ME, Sibly RM, Brown JH. 2010. Shifts in metabolic scaling, production, and efficiency across major evolutionary transitions of life. *Proceedings of the National Academy of Sciences, USA* **107**: 12941–12945.

Dickson AG, Riley JP. 1979. The estimation of acid dissociation constants in seawater media from potentionmetric titrations with strong base. I. The ionic product of water. *Marine Chemistry* **7**: 89–99.

Edwards KF, Thomas MK, Klausmeier CA, Litchman E. 2012. Allometric scaling and taxonomic variation in nutrient utilization traits and maximum growth rate of phytoplankton. *Limnology and Oceanography* **57**: 554–566.

Edwards KF, Thomas MK, Klausmeier CA, Litchman E. 2015. Light and growth in marine phytoplankton: allometric, taxonomic, and environmental variation. *Limnology and Oceanography* **60**: 540–552.

Elzenga JTM, Prins HB, Stefels J. 2000. The role of extracellular carbonic anhydrase activity in inorganic carbon utilization of *Phaeocystis globosa* (Prymnesiophyceae): a comparison with other marine algae using the isotopic disequilibrium technique. *Limnology and Oceanography* **45**: 372–380.

Field CB, Behrenfeld MJ, Randerson JT, Falkowski P. 1998. Primary production of the biosphere: integrating terrestrial and oceanic components. *Science* **281**: 237–240.

Fielding AS, Turpin DH, Guy RD, Calvert SE, Crawford DW, Harrison PJ. 1998. Influence of the carbon concentrating mechanism on carbon stable isotope discrimination by the marine diatom *Thalassiosira pseudonana*. *Canadian Journal of Botany* **76**: 1098–1103.

Finkel ZV, Beardall J, Flynn KJ, Quigg A, Rees TAV, Raven JA. 2010. Phytoplankton in a changing world: cell size and elemental stoichiometry. *Journal of Plankton Research* **32**: 119–137.

Flynn KJ, Raven JA. 2017. What is the limit for photoautotrophic plankton growth rates? *Journal of Plankton Research* **39**: 13–22.

Fogel M, Cifuentes LA, Velinsky DJ, Sharp J. 1992. Relationship of carbon availability in estuarine phytoplankton to isotopic composition. *Marine Ecology Progress Series* **82**: 291–300.

Francois R, Altabet MA, Goericke R, McCorkle DC, Brunnet C, Poisson A. 1993. Changes in the $\delta^{13}C$ of surface water particulate organic matter across the subtropical convergence in the SW Indian Ocean. *Global Biogeochemical Cycles* 7: 627–644.

Friederich GE, Walz PM, Burczynski MG, Chavez FP. 2002. Inorganic carbon in the central California upwelling system during the 1997–1999 El Nino–La Nina event. *Progress in Oceanography* **54**: 185–203.

Fry B. 2006. *Stable isotope ecology, vol. 521*. New York, NY, USA: Springer.

Gardner JL, Peters A, Kearney MR, Joseph L, Heinsohn R. 2011. Declining body size: a third universal response to warming? *Trends in Ecology & Evolution* **26**: 285–291.

Giordano M, Beardall J, Raven JA. 2005. CO_2 concentrating mechanisms in algae: mechanisms, environmental modulation, and evolution. *Annual Review in Plant Biology* **56**: 99–131.

Giordano M, Bowes G. 1997. Gas exchange and C allocation in *Dunaliella salina* cells in response to the N source and CO_2 concentration used for growth. *Plant Physiology* **115**: 1049–1056.

Giordano M, Maberly S. 1989. Distribution of carbonic anhydrase in British marine macroalgae. *Oecologia* **81**: 534–539.

Grover JP. 1989. Influence of cell shape and size on algal competitive ability. *Journal of Phycology* **25**: 402–405.

Guillard RRL. 1975. Culture of phytoplankton for feeding marine invertebrates. In: Smith WL, Chanley MH, eds. *Culture of marine invertebrate animals*. New York, NY, USA: Plenum Press, 26–60.

Heakal FE-T, Hefny MM, El-Tawab AMA. 2010. Electrochemical behavior of 304L stainless steel in high saline and sulphate solutions containing alga *Dunaliella salina* and β-carotene. *Journal of Alloys and Compounds* **491**: 636–642.

Hillebrand H, Dürselen CD, Kirschtel D, Pollingher U, Zohary T. 1999. Biovolume calculation for pelagic and benthic microalgae. *Journal of Phycology* **35**: 403–424.

Hopkinson BM, Dupont CL, Allen AE, Morel FM. 2011. Efficiency of the CO_2-concentrating mechanism of diatoms. *Proceedings of the National Academy of Sciences, USA* **108**: 3830–3837.

Hopkinson BM, Meile C, Shen C. 2013. Quantification of extracellular carbonic anhydrase activity in two marine diatoms and investigation of its role. *Plant Physiology* **162**: 1142–1152.

Hopkinson BM, Young JN, Tansik AL, Binder BJ. 2014. The minimal CO_2-concentrating mechanism of *Prochlorococcus* spp. MED4 is effective and efficient. *Plant Physiology* **166**: 2205–2217.

Huisman J, Weissing F. 1995. Competition for nutrients and light among phytoplankton species in a mixed water column: theoretical studies. *Water Science and Technology* **32**: 143–147.

Iglesias-Rodriguez M, Merrett M. 1997. Dissolved inorganic carbon utilization and the development of extracellular carbonic anhydrase by the marine diatom *Phaeodactylum tricornutum*. *New Phytologist* **135**: 163–168.

Iglesias-Rodriguez M, Nimer N, Merrett M. 1998. Carbon dioxide-concentrating mechanism and the development of extracellular carbonic anhydrase in the marine picoeukaryote *Micromonas pusilla*. *New Phytologist* **140**: 685–690.

Iñiguez C, Capó-Bauçà S, Niinemets Ü, Stoll H, Aguiló-Nicolau P, Galmés J. 2020. Evolutionary trends in Rubisco kinetics and their co-evolution with CO_2 concentrating mechanisms. *The Plant Journal* **101**: 897–918.

Jimenez C, Capasso JM, Edelstein CL, Rivard CJ, Lucia S, Breusegem S, Berl T, Segovia M. 2009. Different ways to die: cell death modes of the unicellular chlorophyte *Dunaliella viridis* exposed to various environmental stresses are mediated by the caspase-like activity DEVDase. *Journal of Experimental Botany* **60**: 815–828.

Johnson KS. 1982. Carbon dioxide hydration and dehydration kinetics in seawater. *Limnology and Oceanography* **27**: 849–855.

Korb RE, Raven JA, Johnston AM, Leftley JW. 1996. Effects of cell size and specific growth rate on stable carbon isotope discrimination by two species of marine diatom. *Marine Ecology Progress Series* **143**: 283–288.

Lee K, Wanninkhof R, Feely RA, Millero FJ, Peng T-H. 2000. Global relationships of total inorganic carbon with temperature and nitrate in surface seawater. *Global Biogeochemical Cycles* **14**: 979–994.

Litchman E, Klausmeier CA. 2008. Trait-based community ecology of phytoplankton. *Annual Review of Ecology, Evolution, and Systematics* **39**: 615–639.

Litchman E, Klausmeier CA, Bossard P. 2004. Phytoplankton nutrient competition under dynamic light regimes. *Limnology and Oceanography* **49** (4part2): 1457–1462.

Lopez-Sandoval DC, Rodriguez-Ramos T, Cermeno P, Sobrino C, Maranon E. 2014. Photosynthesis and respiration in marine phytoplankton: relationship with cell size, taxonomic affiliation, and growth phase. *Journal of Experimental Marine Biology and Ecology* **457**: 151–159.

Maberly SC. 1990. Exogenous sources of inorganic carbon for photosynthesis by marine macroalgae 1. *Journal of Phycology* **26**: 439–449.

Malerba ME, Ghedini G, Marshall DJ. 2020. Genome size affects fitness in the eukaryotic alga *Dunaliella tertiolecta*. *Current Biology* **30**: 3450–3456.

Malerba ME, Marshall DJ. 2019. Size-abundance rules? Evolution decouples body size, energy and demography. *Ecology Letters* **22**: 1407–1416.

Malerba ME, Marshall DJ. 2020. Testing the drivers of the temperature–size covariance using artificial selection. *Evolution* **74**: 169–178.

Malerba ME, Palacios MM, Marshall DJ. 2018a. Do larger individuals cope with resource fluctuations better? An artificial selection approach. *Proceedings of the Royal Society B: Biological Sciences* **285**: 1–9.

Malerba ME, Palacios MM, Palacios Delgado YM, Beardall J, Marshall DJ. 2018b. Cell size, photosynthesis and the package effect: an artificial selection approach. *New Phytologist* **219**: 449–461.

Malerba ME, White CR, Marshall DJ. 2018c. Eco-energetic consequences of evolutionary shifts in body size. *Ecology Letters* **21**: 54–62.

Maranon E. 2015. Cell size as a key determinant of phytoplankton metabolism and community structure. *Annual Review in Marine Science* **7**: 241–264.

Miller AG, Colman B. 1980. Evidence for HCO_3^- transport by the blue-green alga (cyanobacterium) *Coccochloris peniocystis*. *Plant Physiology* **65**: 397–402.

Millero FJ. 2010. Carbonate constants for estuarine waters. *Marine and Freshwater Research* **61**: 139–142.

Miyachi S, Tsuzuki M, Avramova ST. 1983. Utilization modes of inorganic carbon for photosynthesis in various species of *Chlorella*. *Plant Cell Physiology* **24**: 441–451.

Niklas KJ, Cobb ED. 2017. Size-dependent variation in plant form. *Current Biology* **27**: R900–R905.

Nimer N, Guan Q, Merrett M. 1994. Extra-and intra-cellular carbonic anhydrase in relation to culture age in a high-calcifying strain of *Emiliania huxleyi* Lohmann. *New Phytologist* **126**: 601–607.

Pierrot D, Lewis E, Wallace DWR. 2006. MS Excel program developed for CO_2 system calculations. ORNL/CDIAC-105a. Carbon Dioxide Information Analysis Center, Oak Ridge National Laboratory, U.S. Department of Energy, Oak Ridge, TN. doi: https://doi.org/10.3334/CDIAC/otg.CO2SYS_XLS_CDIAC105a

Popp BN, Laws EA, Bidigare RR, Dore JE, Hanson KL, Wakeham SG. 1998. Effect of phytoplankton cell geometry on carbon isotopic fractionation. *Geochimica et Cosmochimica Acta* **62**: 69–77.

Raven JA. 1987. Physiological consequences of extremely small size for autotrophic organisms in the sea. *Photosynthetic Picoplankton* **214**: 1–70.

Raven J. 1998. The twelfth Tansley Lecture. Small is beautiful: the picophytoplankton. *Functional Ecology* **12**: 503–513.

Raven JA. 2009. Carbon dioxide fixation by *Dunaliella* spp. and the possible use of this genus in carbon dioxide mitigation and waste reduction. In: Ben-Amotz A, ed. *The alga* Dunaliella. Boca Raton, FL, USA: CRC Press, 359–384.

Raven JA, Beardall J. 2018. Opportunities for, and limitations on, the functioning of very small cells, illustrated by the Chlorophyta and charophycean Streptophyta. *Perspectives in Phycology* **5**: 1–12.

Raven JA, Beardall J, Giordano M. 2014. Energy costs of carbon concentrating mechanisms in aquatic organisms. *Photosynthesis Research* **121**: 111–124.

Raven J, Beardall J, Sánchez-Baracaldo P. 2017. The possible evolution and future of CO_2-concentrating mechanisms. *Journal of Experimental Botany* **68**: 4761–3716.

Raven JA, Finkel ZV, Irwin AJ. 2005. Picophytoplankton: bottom-up and top-down controls on ecology and evolution. *Vie et Milieu* **55**: 209–215.

Raven JA, Gobler CJ, Hansen PJ. 2020. Dynamic CO_2 and pH levels in coastal, estuarine, and inland waters: theoretical and observed effects on harmful algal blooms. *Harmful Algae* **91**: 101594.

Raven JA, Johnston AM, Kübler JE, Korb R, McInroy SG, Handley LL, Scrimgeour CM, Walker DI, Beardall J, Vanderklift M *et al.* 2002. Mechanistic interpretation of carbon isotope discrimination by marine macroalgae and seagrasses. *Functional Plant Biology* **29**: 355–378.

Raven JA, Knight CA, Beardall J. 2019. Cell size has gene expression and biophysical consequences for cellular function. *Perspectives in Phycology* **6**: 81–94.

Raven JA, Kübler JE. 2002. New light on the scaling of metabolic rate with the size of algae. *Journal of Phycology* **38**: 11–16.

Reinfelder JR. 2011. Carbon concentrating mechanisms in eukaryotic marine phytoplankton. *Annual Review of Marine Science* **3**: 291–315.

Riebesell U, Wolf-Gladrow D, Smetacek V. 1993. Carbon dioxide limitation of marine phytoplankton growth rates. *Nature* **361**: 249–251.

Schindelin J, Arganda-Carreras I, Frise E, Kaynig V, Longair M, Pietzsch T, Preibisch S, Rueden C, Saalfeld S, Schmid B *et al.* 2012. Fiji: an open-source platform for biological-image analysis. *Nature Methods* **9**: 676–682.

Sett S, Schulz KG, Bach LT, Riebesell U. 2018. Shift towards larger diatoms in a natural phytoplankton assemblage under combined high-CO_2 and warming conditions. *Journal of Plankton Research* **40**: 391–406.

Shuter BJ. 1978. Size dependence of phosphorus and nitrogen subsistence quotas in unicellular microorganisms. *Limnology and Oceanography* **23**: 1248–1255.

Sieburth J, Smetacek V, Lenz J. 1978. Pelagic ecosystem structure: heterotrophic compartments of the plankton and their relationship to plankton size fractions. *Limnology and Oceanography* **23**: 1256–1263.

Smith-Harding TJ, Beardall J, Mitchell JG. 2017. The role of external carbonic anhydrase in photosynthesis during growth of the marine diatom *Chaetoceros muelleri*. *Journal of Phycology* **53**: 1159–1170.

Tortell PD. 2000. Evolutionary and ecological perspectives on carbon acquisition in phytoplankton. *Limnology and Oceanography* **45**: 744–750.

Tortell PD, Payne CD, Li Y, Trimborn S, Rost B, Smith WO, Riesselman C, Dunbar RB, Sedwick P, DiTullio GR. 2008. CO_2 sensitivity of Southern Ocean phytoplankton. *Geophysical Research Letters* **35**: 1–5.

Weiss RF. 1974. Carbon dioxide in water and seawater: the solubility of a non-ideal gas. *Marine Chemistry* **2**: 203–215.

Wilbur KM, Anderson NG. 1948. Electrometric and colorimetric determination of carbonic anhydrase. *Journal of Biological Chemistry* **176**: 147–154.

Wolf-Gladrow D, Riebesell U. 1997. Diffusion and reactions in the vicinity of plankton: a refined model for inorganic carbon transport. *Marine Chemistry* **59**: 17–34.

Wu Y, Campbell DA, Irwin AJ, Suggett DJ, Finkel ZV. 2014. Ocean acidification enhances the growth rate of larger diatoms. *Limnology and Oceanography* **59**: 1027–1034.

Yoshiyama K, Mellard JP, Litchman E, Klausmeier CA. 2009. Phytoplankton competition for nutrients and light in a stratified water column. *American Naturalist* **174**: 190–203.

Young EB, Beardall J. 2005. Modulation of photosynthesis and inorganic carbon acquisition in a marine microalga by nitrogen, iron, and light availability. *Canadian Journal of Botany* **83**: 917–928.

Young E, Beardall J, Giordano M. 2001. Inorganic carbon acquisition by *Dunaliella tertiolecta* (Chlorophyta) involves external carbonic anhydrase and direct HCO_3^- utilization insensitive to the anion exchange inhibitor DIDS. *European Journal of Phycology* **36**: 81–88.

Supporting Information

Additional Supporting Information may be found online in the Supporting Information section at the end of the article.

Fig. S1 All three experimental runs for the effects of cell volume on carbon uptake parameters in *Dunaliella tertiolecta*.

Table S1 Replicates used in each assay for each size-selection treatment of *Dunaliella tertiolecta*.

Please note: Wiley Blackwell are not responsible for the content or functionality of any Supporting Information supplied by the authors. Any queries (other than missing material) should be directed to the *New Phytologist* Central Office.